Influence of Photopolymerization Reaction Kinetics on Diffraction Efficiency of H-PDLC Undergoing Photopatterning Reaction in Mixtures of Acrylic Monomer/Nematic Liquid Crystals

Scott Meng,[†] Hatice Duran,[†] Jun Hu,[‡] Thein Kyu,*[,†] Lalgudi V. Natarajan,[§] Vincent P. Tondiglia,[§] Richard L. Sutherland,[⊥] and Timothy J. Bunning[⊥]

Department of Polymer Engineering, University of Akron, Akron, Ohio 44325-0301; Department of Chemistry, University of Akron, Akron, Ohio 44325-3601; Science Applications International Corporation, Dayton, Ohio 45431; and Air Force Research Laboratory, Materials and Manufacturing Directorate, Wright-Patterson Air Force Base, Ohio 45433

Received January 17, 2007; Revised Manuscript Received March 9, 2007

ABSTRACT: The influence of photopolymerization reaction kinetics on diffraction efficiency has been investigated on the mixtures of photocurable acrylic monomer/nematic liquid crystals subjected to photopatterning. Photodifferential scanning calorimetry and real-time Fourier transform infrared spectroscopy experiments were conducted as a function of concentration in order to determine the reaction kinetics of acrylic monomer/liquid crystal mixtures. The lumped reaction rate constants for each concentration exhibited a nonlinear variation of the reaction rate constant with conversion and concentration. To gain fundamental insight, theoretical modeling and numerical simulation have been carried out by combining Flory−Huggins free energy of isotropic mixing and Maier−Saupe free energy of nematic ordering in conjunction with the experimentally determined reaction rate constants. The evolution of diffraction efficiency is discussed in terms of photopolymerization rates, monomer concentrations, and also the type of diffusion such as Fick diffusion occurring in a single phase or mutual diffusion in phase separating systems.

Introduction

Photopolymerization techniques have been customarily applied to coatings, electro-optical devices, contact lenses, and dental restoration, among others.[1−11] This technique has been extended to holographic lithography and photopatterning.[10,11] Holographic photopolymerization operates on the basis of principles of wave interference of coherent light to realize a spatially modulated photopattern at a submicron length scale. With appropriate polarized beam geometries, various interference patterns may be imprinted onto a mixture of liquid crystal (LC) and photoreactive monomer as a means of fabricating electrically switchable holographic polymer dispersed liquid crystals (H-PDLC) and polymeric photonic crystals. In addition to photocurable monomer and nonreactive nematic liquid crystals (e.g., cyanobiphenyl derivatives), the photocurative mixtures contain photoinitiators and cocatalysts. Most of the photocurable monomers used in practice were acrylate derivatives because of their fast curing rate and chemical versatility including multiarm acrylate.

The structure and electro-optical performance of the H-PDLC as well as photonic crystals are controlled by the competition between photopolymerization kinetics and phase separation dynamics.[12,13] The photopolymerization kinetics has been customarily determined by means of photodifferential scanning calorimetry (P-DSC)[14−17] and real-time Fourier transform infrared spectroscopy (FTIR).[18,19] Decker and co-workers[20] applied the real-time infrared (RT-IR) technique to the investigation of the photopolymerization kinetics of mono- and multiacrylate monomers under continuous laser illumination at 368.3 nm. It was demonstrated that the RT-IR approach was capable of following the kinetics of photopolymerization in a fraction of a second. Recently, Lee et al. employed the real-time FTIR to investigate the photopolymerization kinetics of vinyl acrylate by probing characteristic absorption peaks of acrylate and vinyl groups.[21] They found that the acrylate groups of vinyl acrylate react faster than conventional acrylic monomers.

From a theoretical prospective, Schultz et al. deduced an analytical expression for modeling the reaction kinetics of photopolymerization to a first approximation, assuming termination through bimolecular combination.[22,23] Subsequently, Wen and McCormick[24] modified the above kinetic model by taking into account the radical trapping in photopolymerization of multifunctional monomers. Under the assumption that the trapping rate constant increased exponentially as a function of the inverse of free volume, their model captured the experimental trends that the active radical concentration passed through a maximum while trapped radical concentration increased monotonically. Perry and co-workers further considered the attenuation effect by the sample thickness, showing the strong dependence of the critical cure depth on the light intensity for a given photoinitiator concentration.[25]

In a comprehensive photopolymerization kinetic model of Goodner and Bowman, the effects of mass transfer and heat transfer were incorporated in the model, allowing variation of temperature, concentration, and light intensity through the thickness of the thick film.[26] The primary radical termination and inhibition were included in the termination step. It was reported that the reaction heat generated in the thick films brought about an appreciably higher conversion. Furthermore, Guymon and Bowman examined the photopolymerization kinetics via P-DSC in a ferroelectric liquid crystalline medium containing mesogenic and nonmesogenic diacrylate monomers

* Corresponding author. E-mail: tkyu@uakron.edu.
[†] Department of Polymer Engineering, University of Akron.
[‡] Department of Chemistry, University of Akron.
[§] Science Applications International Corporation.
[⊥] Air Force Research Laboratory.

10.1021/ma070135q CCC: $37.00
Published on Web 04/05/2007

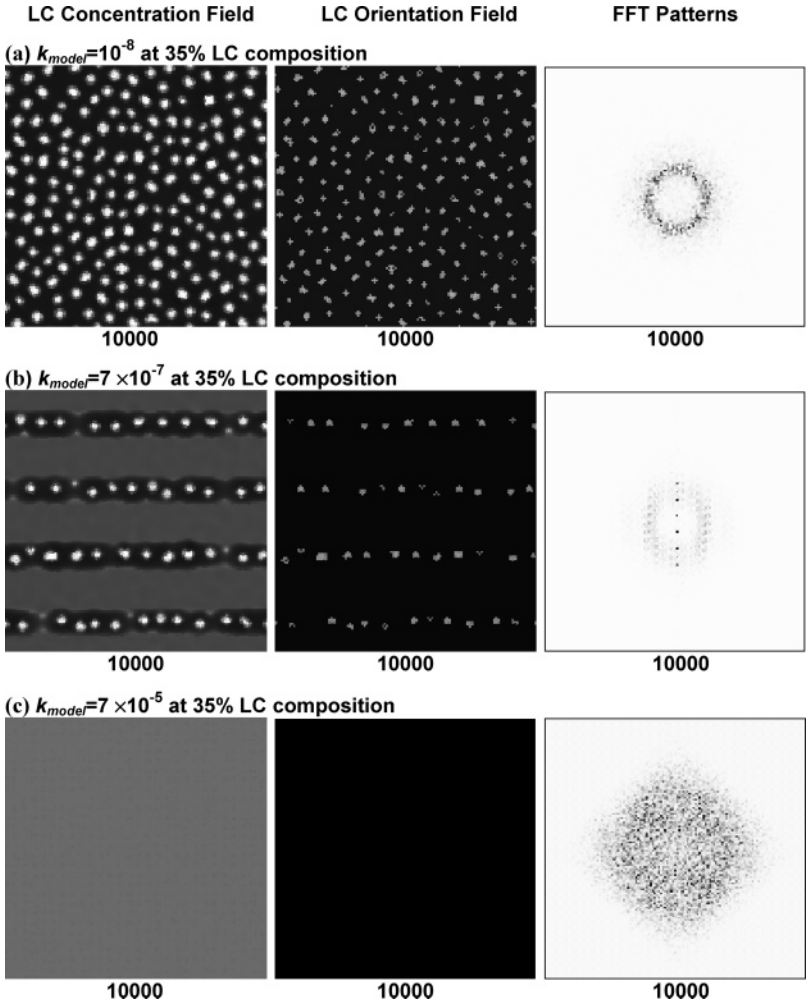

Figure 1. Comparison of $D_m = 0.01$ and $D_{LC} = 2$ with difference of the apparent reaction kinetic constant (a) $k_{model} = 10^{-8}$, (b) $k_{model} = 7 \times 10^{-7}$, and (c) $k_{model} = 7 \times 10^{-5}$ at 35% LC composition.

at different temperatures and under different LC phases.[27] It was revealed that the photopolymerization kinetics can be drastically influenced by temperature as well as by the types of the LC phases. On the basis of a linear relationship assumption between refractive index and conversion of double bonds, Carre et al. employed holography for investigating the photopolymerization mechanisms and kinetics in the system containing mono- and difunctional acrylamide and its derivatives.[28] Using a combined theoretical and experimental approach, they analyzed the process of hologram formation on the basis of the temporal evolution of diffraction efficiency assuming that the polymerization rate was proportional to the square root of the intensity.

In a previous paper, we reported how the composition of monomer/LC affects the progression of diffraction efficiency (DE) during the formation of H-PDLC via pattern photopolymerizing mixtures of acrylic monomer/nematic (LC) in reference to the phase diagram of the starting mixture.[29] At that time, we focused on the diffusion aspect of a reaction−diffusion process, i.e., H-PDLC formation. In this paper, we emphasize the reaction aspect by exploring how the photopolymerization reaction kinetics quantitatively affects the progression of DE. The present work combines experimental reaction kinetic studies in conjunction with theoretical modeling and simulation. Our theoretical modeling was developed in the framework of the Ginzburg−Landau model C equation, pertaining to the spatiotemporal evolution of the conserved LC concentration order parameter and nonconserved LC orientation order parameter coupled with the reaction kinetic equation. We combined the local free energy of the Flory−Huggins free energy of isotropic mixing and the Maier−Saupe free energy of nematic ordering. The photopolymerization kinetics of the mixture of acrylic monomer/LC was monitored by means of photodifferential scanning calorimetry as well as by real-time Fourier transformed infrared spectroscopy. On the basis of our previously developed model that links the DE evolution with the structural development of H-PDLC, the simulation utilizes the experimentally measured time-dependent and concentration-dependent reaction kinetic constants to decipher the effect of reaction kinetics on the DE during H-PDLC fabrication.

Experiments

The multifunctional monomer, pentaerythritol tetraacrylate, was purchased from Aldrich Chemical Corp. The eutectic cyanobiphenyl nematic liquid crystal (E7) was purchased from Merck Chemical Co., having a reported nematic−isotropic transition temperature of 60 °C. All materials were used as received without further purification.

The syrup for photopolymerization was prepared by mixing tetraacrylate with initiator (Rose Bengal derivative), co-initiator (*N*-phenylglycine), solubilizing agent (*N*-vinylpyrrolidone), and surfactant (octanoic acid), according to a recipe reported elsewhere.[30] The syrup was mixed thoroughly for 24 h and then poured directly into P-DSC pans for the P-DSC experiments. The individual sample was weighed after equilibrating at 25 °C isothermally in nitrogen environment. The photo-DSC instrument (Thermal Advantage Instruments, Q series) was operated at the UV wavelength of 360

nm and 22 mW/cm^2. All samples were illuminated under uniform UV radiation for various exposure times. The reaction heat flow vs time data were collected to establish the trends of the lumped reaction kinetic constant (k) vs reaction time.

In the FTIR experiments, green laser light (operated at the wavelength of 532 and nm 20 mW/cm^2) was illuminated on the photocurable syrup film that was uniformly coated on a prism surface. The whole chamber of the FTIR instrument (Nexus 870, Thermo Spectra Tech) was purged with nitrogen gas circulation. After subtracting the background, each infrared absorption spectrum thus acquired under continuous irradiation was the average of 30 scans.[21] The Rose Bengal photoinitiator possesses two absorption peaks near 365 and 532 nm; their ratio is about approximately 2:1, which was already accounted for in our calibration.[30] Moreover, the different wavelengths used in P-DSC and FTIR experiments may be calibrated in accordance with the absorption spectrum of Rose Bengal to validate the comparison of the apparent reaction kinetics vs time curves obtained by the above two methods.

The reflection grating fabrication process was probed by means of a He−Ne laser (633 nm and 5 mW/cm^2). The diffraction efficiency (DE) of reflection gratings was monitored using a fiber-optic spectrometer (Ocean Optics) within an operating range of 350−1000 nm and a resolution of ~1.5 nm. The detailed experimental setup for photopatterning the reflection grating and monitoring the DE evolution may be found elsewhere.[32]

Models and Simulation Scheme

H-PDLC Pattern Formation. The total free energy of the tetraacrylate/E7 system, G, may be described in terms of the integral of local free energy densities and the nonlocal gradients over all volume[29]

$$G = \int_V (g^{\mathrm{i}} + g^{\mathrm{n}} + \kappa_\phi |\nabla\phi|^2 + \kappa_s |\nabla s|^2)\, \mathrm{d}V \tag{1}$$

where g^{i} and g^{n} are the local Flory−Huggins free energy density of isotropic mixing and Maier−Saupe free energy density of nematic ordering, respectively. The Flory−Huggins free energy of isotropic mixing for the monomer/LC system is given as[33−35]

$$g^{\mathrm{i}} = (\phi_{\mathrm{LC}}/r_{\mathrm{LC}}) \ln \phi_{\mathrm{LC}} + ((1-\phi_{\mathrm{LC}})/r_{\mathrm{m}}) \ln(1-\phi_{\mathrm{LC}}) + \chi\phi_{\mathrm{LC}}(1-\phi_{\mathrm{LC}}) \tag{2}$$

where ϕ_{LC} represents the volume fraction of LC in the mixture and χ is the FH interaction parameter. r_{LC} and r_{m} are the respective degree of polymerization of LC and monomer, and both are taken as unity at the onset of polymerization in this study. The Maier−Saupe free energy density of nematic ordering is written as follows:[35,36]

$$g^{\mathrm{n}} = \frac{1}{r_{\mathrm{LC}}}\left(-\phi_{\mathrm{LC}} \ln z + \frac{1}{2}\nu\phi_{\mathrm{LC}}{}^2 s^2\right) \tag{3}$$

In eq 3, s is the orientation order parameter, defined as $s = (3\langle\cos^2\theta\rangle - 1)/2$, θ being the angle between the LC director and the reference axis. z is the partition function, and ν stands for the nematic interaction parameter and takes the form $\nu = 4.541 T_{\mathrm{NI}}/T$, in which T_{NI} is the nematic−isotropic transition temperature of LC.

To mimic the spatiotemporal growth of H−PDLC structure, G is incorporated into the time dependent Ginzburg−Landau equations as[29]

$$\frac{\partial\phi_{\mathrm{LC}}(r,t)}{\partial t} = \nabla\cdot\left[\Lambda\nabla\left(\frac{\delta G}{\delta\phi_{\mathrm{LC}}}\right)\right] \tag{4}$$

$$\frac{\partial\phi_{\mathrm{m}}(r,t)}{\partial t} = \nabla\cdot\left[\Lambda\nabla\left(\frac{\delta G}{\delta\phi_{\mathrm{m}}}\right)\right] - k\left[1 + V_{\mathrm{F}}\cos\left(\frac{2\pi x}{L}N_x\right)\right]\phi_{\mathrm{m}} \tag{5}$$

$$\frac{\partial\phi_{\mathrm{p}}(r,t)}{\partial t} = k\left[1 + V_{\mathrm{F}}\cos\left(\frac{2\pi x}{L}N_x\right)\right]\phi_{\mathrm{m}} \tag{6}$$

and

$$\frac{\partial s(r,t)}{\partial t} = -R_s\left(\frac{\delta G}{\delta s}\right) \tag{7}$$

In the above equations, ϕ_{m} and ϕ_{p} stand for the volume fraction of monomer and polymer, respectively, with $\phi_{\mathrm{LC}} + \phi_{\mathrm{m}} + \phi_{\mathrm{p}} = 1$. V_{F} stands for the visibility factor. Λ is the mutual diffusion coefficient among reactive monomer, emerging polymer, and LC, while R_s represents the rotational mobility of LC directors. k is the apparent reaction kinetic constant to be introduced latter. Our previous experimental results showed that only two coexisting phases (e.g., liquid crystal-rich, liquid crystal-lean) were observable,[11] which in turn validates the treatment of the present case as a pseudo-two-phase system. The reference system for the simulation is a multifunctional photoreactive monomer (e.g., tetraacrylate) and nematic liquid crystal (E7). The spatiotemporal evolution of the concentration/orientation order parameters of monomer and/or LC have been simulated according to eqs 4−7 by employing a finite central difference method for spatial steps and an explicit forward difference method for time steps under periodic boundary conditions on a 128 × 128 grid. To ensure the stability of the simulation, different grid sizes and time steps have been utilized.

Apparent Reaction Kinetic Constant Determination. In eq 5, k symbolizes the apparent reaction kinetic constant in the form of a lumped constant of k_{p}, k_{t}, and I_{a}[30]

$$k = \frac{k_{\mathrm{p}}}{k_{\mathrm{t}}^{1/2}}(k_{\mathrm{e}}^{1/2}\Phi^{u} I_{\mathrm{a}}^{u}) \tag{8}$$

where Φ represents the quantum efficiency, k_{e} the coefficient of photoradical generation, and I_{a} the absorbed intensity of light. k_{p} and k_{t} are the reaction rate constants of propagation and termination, respectively. For classical radical polymerization, the exponent of absorbed intensity would be $u = 1/2$. In bulk or concentrated solution polymerization this relationship applies only to the initial phase of the reaction.[1,30] As soon as termination by trapping competes with termination by combination, the intensity exponent will increase to unity. The exponent of unity was used here because of the steady-state assumption adopted in the simulation. It should be pointed out that our simulation based on the above-mentioned correlation of $k = I_{\mathrm{a}}^{1/2}$ failed to account for the experimental sinusoidal concentration profiles developed at the initial stage of the grating formation;[29,30] the correlation of $k = I_{\mathrm{a}}$ was needed to capture this sinusoidal variation. The apparent reaction kinetic constant may be extrapolated from P-DSC experiment via the analysis of the heat flow vs time curve on the basis of the following equations[22]

$$\frac{\mathrm{d}\alpha}{\mathrm{d}t} = (1-\alpha)k = \frac{1}{\Delta H^{\circ}_{\mathrm{m}}}\frac{\mathrm{d}H}{\mathrm{d}t} \tag{9}$$

where α represents the conversion of acrylic monomers, $\Delta H^{\circ}_{\mathrm{m}}$ stands for the heat of polymerization of acrylic monomers, and $\mathrm{d}H/\mathrm{d}t$ is the differential heat flow from P-DSC. A literature value of $\Delta H^{\circ}_{\mathrm{m}} = 86.1$ kJ/mol was used as the heat generated during

the photoreaction of acrylic double bonds.[37] The C=C double bond conversion α may be obtained by integrating the area under the heat flow vs time curve normalized by a reference literature value of the 100% conversion. The apparent reaction kinetic constant may be determined in accordance with eqs 9 and 10. Correspondingly, plotting the k determined at different times renders the apparent reaction kinetic constant vs time curves.

The apparent reaction kinetic constant may also be extrapolated from the FTIR experiment by monitoring the evolution of the characteristic absorbance of certain functional groups such as acrylate band at 1635 cm^{-1}. The conversion of the acrylate group can be calculated according to[21]

$$\alpha = \frac{A_0 - A_t}{A_0} \tag{10}$$

where A_0 and A_t represent the absorbance at time zero and at time t, respectively. The acrylic double bond conversion vs time curve was drawn from the decaying acrylic group absorption peak divided by the initial absorbance peak for various times. To obtain the differential conversion rate $d\alpha/dt$, the conversion vs time curve was curve-fitted by means of Taylor expansion. After that, the differential conversion rate at a specific time may be calculated by taking the first derivative of the fitted Taylor expansion at each specific time. In a similar manner, the time-dependent apparent reaction kinetic constant may be obtained in accordance with eq 9.

Diffraction Efficiency Evolution. H-PDLC is composed of LC-rich and LC-lean striations. Once the compositions of liquid crystal and monomer in LC-rich and LC-lean stripes are determined, the s-polarized diffraction efficiency η of an ideal, unslanted H-PDLC film may be evaluated in accordance with the following equation:[29,38−41]

$$\eta = \delta_a \tanh^2\left(\frac{\pi \Delta n_j(t) l}{\lambda \cos \theta_B}\right) \quad (j = s, p) \tag{11}$$

where δ_a is a correction parameter depending upon the ratio of diffraction and scattering from the structural inhomogeneity. λ is the wavelength of the probe beam and θ_B the Bragg angle. $\Delta n_j(t)$ represents the refractive index modulation. For s-polarization[29,40]

$$\Delta n_s(t) = n_{a,yy}^{(1)}(t) - n_{a,yy}^{(1)}(0) \tag{12}$$

In the case of p-polarization

$$\Delta n_p(t) = n_{a,zz}^{(1)}(t) \cos(2\theta_B) + [n_{a,zz}^{(1)}(t) - n_{a,xx}^{(1)}(t)] \sin^2 \theta_B \tag{13}$$

where $n_{a,xx}^{(1)}$, $n_{a,yy}^{(1)}$, and $n_{a,zz}^{(1)}$ are the refractive index components derived from the dielectric tensor. The details of the DE calculation may be found in an earlier paper.[29]

Results and Discussion

As shown in Figure 1, the theoretical simulation provides guidance to the experiments on how the apparent reaction kinetic constant could affect the morphologies formed during H-PDLC fabrication via holographic lithography. The simulation based on model parameters offers qualitative but quick predictions of morphologies and electro-optical properties of the H-PDLC. Figure 1 depicts various distinctive morphologies of the LC domains simulated during the formation of H-PDLC under different model parameters of apparent reaction kinetic constants, according to eqs 4−7. These model parameters for apparent reaction kinetic constants k_{model} were all chosen, in this particular simulation, as fixed values that were neither time-dependent nor concentration-dependent for the sake of comparison. In practice, k_{model} value could be varied by changing the writing beam intensities.

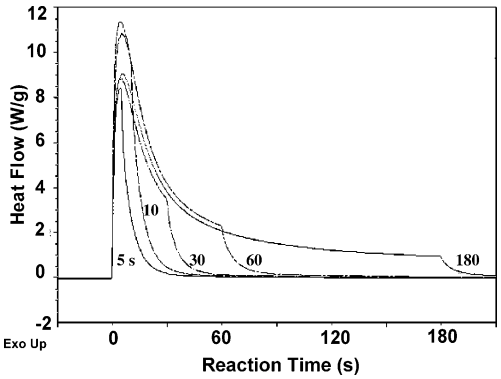

Figure 2. Photo-DSC traces of 100% tetraacrylate system irradiated for 5, 10, 30, 60, and 180 s.

In the case of high intensity of irradiation ($k_{model} = 7 \times 10^{-5}$) in Figure 1, no identifiable structures are discerned in both the concentration and orientation fields, which may be attributed to the fact that the reaction kinetics is so fast that the LC molecules would not have sufficient time to diffuse away into the low-intensity region before being entrapped by the chemical cross-linked networks. Although the translational motions of LC molecules may be greatly hindered due to the chemical junctions, these LC mesogens can still undergo local motions.

In the other extreme case of the low intensity of irradiation ($k_{model} = 10^{-8}$), only a classic "Swiss cheese" PDLC morphology forms without any holographic stripes. The scattering halos in the corresponding Fourier transformed patterns arise from the interparticle interference and reveal no diffraction patterns corresponding to the stratified structures, which manifest themselves that the patterns formed under the very weak interference irradiation closely resemble to the PDLC structures formed under the uniform irradiation.

At an intermediate intensity range ($k_{model} = 7 \times 10^{-7}$), the emergence of the H-PDLC grating may be witnessed in the concentration field. The corresponding diffraction spots from these fringe patterns are evident in the Fourier transformed patterns while suppressing the undesired scattering halo. Apparently, the optimum condition to fabricate H-PDLC would be at the intermediate intensity range.[11,29] It may be inferred that the H-PDLC morphology may be controlled by the apparent reaction kinetic constant via its dependence on interference beam intensities.

In practice, there is no exact way of determining how the apparent reaction kinetic constants at a given experimental condition vary locally in a manner dependent on conversion and concentration. In this work, we determine the reaction rate constants as a function of conversion. Since the local concentration fluctuation evolves with the progression of the reaction, the local reaction rate constants may be estimated through the local monomer or polymer concentration.

P-DSC experiments were conducted to measure the apparent reaction kinetic constants. Figure 2 depicts the evolution of the reaction heat generated under 5, 10, 30, 60, and 180 s of irradiation of the pure tetraacrylate sample. As can be seen in Figure 2, the P-DSC curve shoots up to the maximum heat flow within a few seconds due to the onset of autoacceleration. After reaching the peak value, it decays rapidly with the progression of the termination reaction. The amount of heat generated

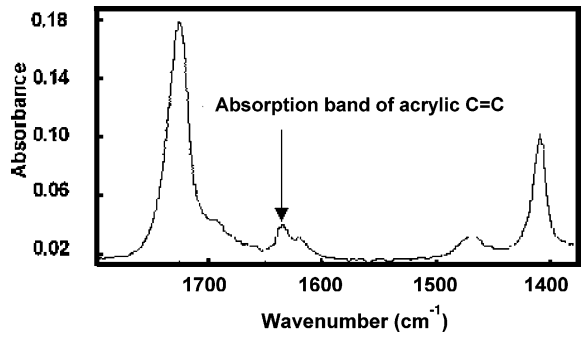

Figure 3. FTIR spectra of tetraacrylate before photopolymerization showing the absorbance at 1635 cm^{-1} assigned to the C═C bond stretching of tetraacrylate.

depends on the entire integrated area under the curve. It is noticed that when the illumination was turned off, all the DSC curves level off within a minute, indicating some traces of the dark reaction. This finding is in line with the observation reported by Lee et al. for the photopolymerization of the vinyl acrylate system.[21]

To cross-check the trend of the P-DSC results, FTIR experiments were conducted in the neat tetraacrylate sample. Figure 3 illustrates the FTIR spectrum of the tetraacrylate at time zero in which 1635 cm^{-1} may be assigned to the C═C double bond stretching of the acrylate group. The depletion of absorption peak at 1635 cm^{-1} was monitored as a function of radiation time during the progression of photopolymerization. As in the case of P-DSC, the autoaccelaration probably occurs, but the average time for 30 scans was not fast enough to discern the autoaccelaration process in the FTIR run; therefore, the initial rise in the absorbance might have been missed. Instead, the absorbance declines rapidly from its maximum value within a few seconds, and eventually it levels off at longer times, displaying a similar trend of the P-DSC experiments, except for the autoacceleration part.

Figure 4a shows the comparison of the apparent reaction kinetic constant vs time curves for various blends as obtained by the P-DSC and FTIR techniques. To decipher the difference in the wavelength of the incident light utilized in the P-DSC and FTIR experiments, the reaction kinetic constants from P-DSC experiments have been normalized on the basis of the absorbance at 365 and 532 nm of the Rose Bengal photoinitiator.[31] After the normalization, both the reaction kinetic constants measured from the P-DSC thermograms and FTIR spectra display a comparable trend having reasonably close values (within 10%). The apparent reaction kinetic constant thus determined from the two methods, although not perfect, turns out to be in reasonably good agreement.

Since the reaction kinetic constant varies with reaction time, it is important to correlate it to the local concentration that also changes with reaction time. In other words, the local reaction kinetic constants may be evaluated through the local concentrations evolving with the progression of the reaction. Figure 4b exhibits the experimentally determined apparent kinetic constants for 5%, 35%, and 50% LC concentrations from the P-DSC experiments. The time-dependent apparent kinetic constants in 5%, 35%, and 50% LC concentrations show the similar trend of the photo reaction to that of the pure tetraacrylate sample in Figure 3a. It may be noticed from Figure 4b that the maximum peak of reaction kinetic constants increases as a function of LC concentration, which is certainly counterintuitive. However, this observed trend may be explicable in terms of mobility enhancement due to the LC. That is to say, the increase of reaction

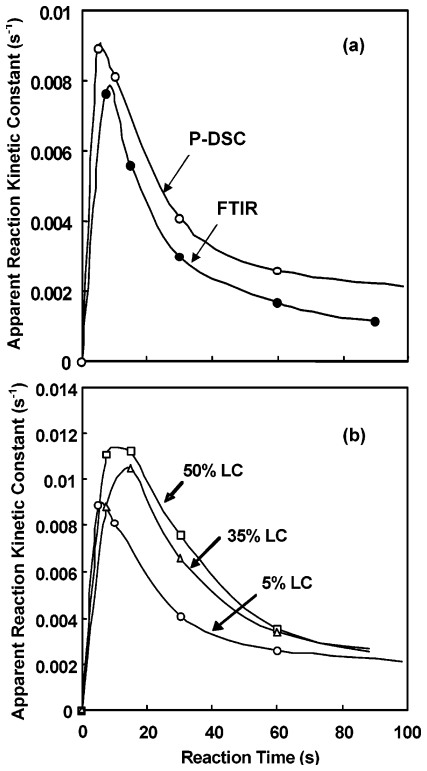

Figure 4. (a) Apparent reaction kinetic constant vs time calculated from the conversion of P-DSC experiments (open symbols) and of real-time FTIR (solid symbols) based on the change in the absorbance at 1635 cm^{-1} normalized by its initial value at time zero. (b) Apparent reaction kinetic constant vs time measured by P-DSC experiments in 5% LC/monomer sample (open circles), 35% LC/monomer sample (open triangles), and 50% LC/monomer sample (open squares).

kinetic constants as a function of LC concentration suggests that in the tetraacrylate/LC mixture the LC molecules lubricate the viscous tetraacrylate component (10^{-11}−10^{-10} cm^2/s), expediting the diffusion of monomers/reacting chains, thereby promoting chain propagation during the course of photopolymerization.

It should be noted that polymerization induced phase separation may be dominant in tetraacrylate/LC that occurs in 35% and 50% LC concentrations. When the average size of the phase separated domains reach the length scale comparable to or larger than the wavelength of the radiation, it attenuates the incident IR beams by virtue of the fact that sample becomes turbid, and thus the Beer−Lambert law may no longer be satisfied. This in turn suggests that FTIR encounters some limitations in the measurement of the apparent kinetic constants, especially for the phase-separating tetraacrylate/LC system.

On the basis of the P-DSC and FTIR observations, it is obvious that the apparent reaction kinetic constant should be treated as both time and concentration dependent. Consequently, it is imperative to reexamine the simulated results of the time-independent apparent kinetic constant by comparing the trends of the temporal evolution diffraction efficiency during the H-PDLC formation for the time-independent apparent kinetic constants vs the aforementioned time- and concentration-dependent variable.

To correlate the morphology development of the H-PDLC to the diffraction efficiency, a theoretical model based on the coupled wave theory was proposed in an earlier publication.[29] To make the comparison on the same scale between the time-independent model apparent reaction kinetic constant and the time- and concentration-dependent ones, the dimensionless

model apparent reaction kinetic constant may be renormalized to the real unit via the relationship

$$k_{\text{model}} = (l_c^2/D_{\text{re}})k \tag{14}$$

where k signifies the apparent reaction kinetic constant in the unit of s^{-1} and D_{re} the reference diffusion coefficient. l_c is the characteristic length of the system. In our reference system (tetraacrylate and E7), the characteristic length is roughly 30−50 nm and the reference diffusion coefficient is $\sim 10^{-8}$ cm^2/s. For the model parameter used in the simulation in Figure 2 ($k_{\text{model}} = 7 \times 10^{-7}$), the renormalized k is around 0.001 s^{-1}, which falls within the range of experimentally determined reaction kinetic constants in Figure 4b, suggesting that our simulation should be quite reasonable.

In the past, k_{model} was treated as a constant parameter; i.e., it is neither time nor space dependent. However, as demonstrated in Figure 4, the experimentally determined apparent reaction kinetic constant $k_{\text{exp}}(t,\phi)$ shows a strong dependency on concentration and also changes with reaction time and therefore with conversion. Although FTIR imaging instrument has become available for characterizing the local concentration of phase separated polymer domains directly, such an instrument is not fast enough to determine the local reaction kinetic constant of fast photopolymerization.

An alternative approach is to make use of the results in Figure 4 that exhibits the variation of the global reaction kinetic constant with reaction time (analogous to conversion) for various concentrations. All P-DSC curves in Figure 4 were further deduced on a surface plot of $k(t,\phi)$ based on the Taylor expansion. By matching with the surface profiles of the local concentration field of the simulation, the dependence of k on t and ϕ may be determined. Evidently, the more experimental P-DSC curves are available, the better the precision would be in constructing the surface plot of $k(t,\phi)$. With the progression of the reaction, the local concentrations are practically tractable in the simulation, and thus the local reaction rate constant may be evaluated through this experimental surface plot of t and ϕ. Despite its very rough approximation, the present approach is still more realistic than the constant k value employed before.[29]

In the previous papers,[29,30] three types of reaction−diffusion were explained for the H-PDLC formation in relation to the different regions of the starting phase diagram. Under those circumstances, simulations were carried out on the basisi of a constant model parameter of reaction kinetics. It is of practical importance to examine whether the constant model parameter is an oversimplification or close to the reality. Figure 5a−c displays the comparison between the temporal evolution of the simulated diffraction efficiencies using a constant ($k_{\text{model}} = 7 \times 10^{-7}$) and the apparent reaction kinetic constant $k_{\text{exp}}(t,\phi)$ for three compositions of 50%, 35%, and 5% liquid crystals. Each composition of monomer corresponds to a distinct diffusion mechanism of H-PDLC fabrication governed by the established phase diagram.[29] At the 5% LC concentration, the system always remains in the single-phase region during the course of photopolymerization, and thus the diffusion in that region is merely a transport-controlled phenomenon. At the 35% LC concentration, the system is thrust into the metastable region upon photoreaction, and the diffusion in that region is mainly driven by thermodynamic driving force via nucleation and growth. In the case of 50% liquid crystals, the system enters the unstable region upon photoreaction, and the phase separation in that region proceeds via spinodal decomposition.

As demonstrated earlier, the 5% LC concentration gives rise to an isotropic grating without undergoing nematic ordering.[29]

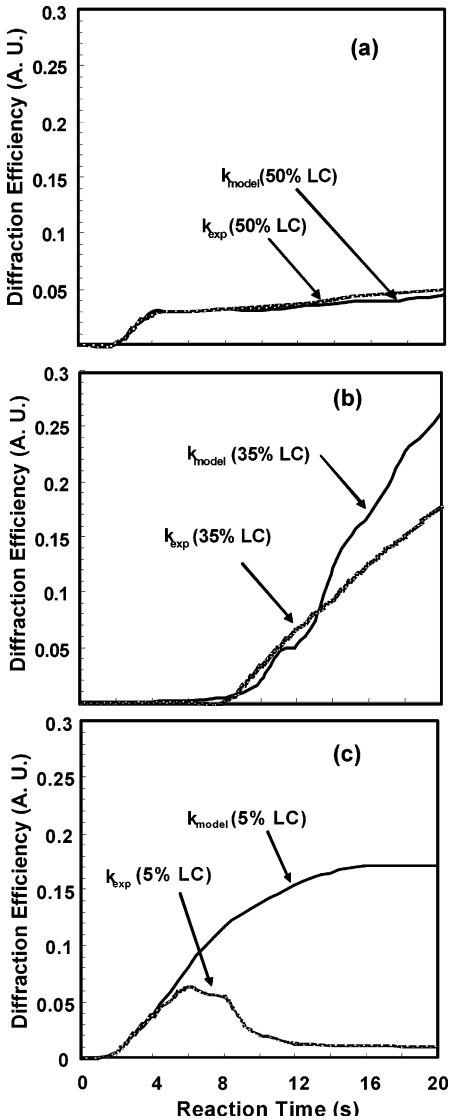

Figure 5. Comparison between the s-polarized DE evolution based on the experimental determined apparent kinetic coefficient k_{exp} and that based on the constant model parameter k_{model} in 35% (a), 50% (b), and 5% (c) LC concentration samples.

No phase separation and thus no p-polarized DE was observed in these 5% LC samples. To keep the consistency in the comparison, we now focus our attention on the s-polarized DE that persists in all 5%, 35%, and 50% LC samples. It may be inferred that the s-polarized DE comes from the *y*-components of refractive index contrast of the LC-rich and LC-lean stripes.[32,40]

To make our simulated results more practical, the simulation time steps were converted back to the real time unit in accordance with the following relationship:

$$t' = (D_{\text{re}}/l_c^2)t \tag{15}$$

where t' stand for the simulation time steps and t the real time. In Figure 5b is shown the s-polarized DE evolution in the 35% LC concentration sample based on the k_{model}, which initially shows no significant increase and stays at a low value (less than 1%) until 7 s later. Subsequently, the s-polarized DE value increases significantly (more than 25%) within 20 s. The induction period of the s-polarized DE corresponds to the stage in which the LC molecules begin to diffuse from low-intensity regions to high-intensity regions. With the progression of the

photopatterning, the LC-rich and the LC-lean stripes are formed in the cured tetraacrylate/LC mixture. Concurrently, phase separation takes place within these preformed LC-rich stripes, revealing numerous heterogeneous LC droplets structures. The interdomain interference arising from the heterogeneous droplet structures causes the scattering of light. The overall s-polarized DE is a consequence of the contributions arising from both scattering and diffraction of these LC stripes.

In Figure 5a, the s-polarized DE in the 50% LC sample based on the k_{model} value rises to 3−4% within the initial period of 4 s and thereafter levels off. The small magnitude of the s-polarized DE in the 50% LC sample is may be attributed to the strong scattering from the phase-separated structures. Comparing the simulated DE based on k_{model} and $k_{exp}(t,\phi)$ in Figure 5a,b, the growth trends are similar for both the 50% and the 35% LC samples. The negligible difference of the s-polarized DE between k_{model} and $k_{exp}(t,\phi)$ in the 50% LC sample implies that the dynamics of phase separation via spinodal decomposition is dominant over the reaction kinetic in the unstable region; therefore, the values of the k_{model} and $k_{exp}(t,\phi)$ make little or no effect on the DE. On the same token, the influence of reaction kinetic on the simulated DE may be insignificant in the 5% LC sample although the mechanism of phase separation is different for the two concentrations. It is reasonable to conclude that the reaction kinetic values may be important especially when the reaction kinetics is dominant over the phase separation kinetics.

In support of the above hypothesis, the comparison of DE evolution between the simulation with k_{model} and $k_{exp}(t,\phi)$ values has been made for the 5% LC sample. As demonstrated in Figure 5c, the DE evolution in 5% LC sample based on k_{model} shows a gradual growth of DE until 14 s, and after that, DE saturates out at the limiting value of 15%. However, in the case of the experimentally determined $k_{exp}(t,\phi)$, the DE evolution in 5% LC sample initially increases and reaches the maximum within 6 s, and subsequently it decays monotonically to a value of 1% and levels off, resembling the evolution of experimental apparent kinetic constant in Figure 4b. The DE evolution predictions based on k_{model} and $k_{exp}(t,\phi)$ are significantly different. This drastic difference manifests that the constant k_{model} may be an oversimplification for this type of Fick diffusion process which is valid only in the single component system or in the miscible system.

From Figure 5, it may be inferred that the nature of the type of diffusion plays an important role in determining the influence of reaction kinetic on diffusion. The Fick diffusion is a simple transport phenomenon that is driven by spatial concentration variation created by pattern photopolymerization. However, such Fick diffusion is valid only in the non-phase-separating system. On the contrary, the mutual diffusion via nucleation and growth or spinodal decomposition is driven by thermodynamic driving force for segregation subjected to photopolymerization which dominates over the reaction kinetics. Hence, the influence of local reaction kinetic rate constant, k_{model} or $k_{exp}(t,\phi)$, even if it exerts some influence on the DE progression, can no longer be discerned here due to the dominance by the phase separation process.

To further examine the validity of simulated DE result in the 95% monomer composition, the simulated DE evolution in the 5% LC sample based on the experimentally determined apparent reaction kinetic constant is compared with the experimentally determined DE trends of the 5% LC sample in Figure 6a,b. The details of the DE experiments were disclosed elsewhere.[40] It may be inferred that our simulation accords well with the experimentally measured reaction kinetic constants and

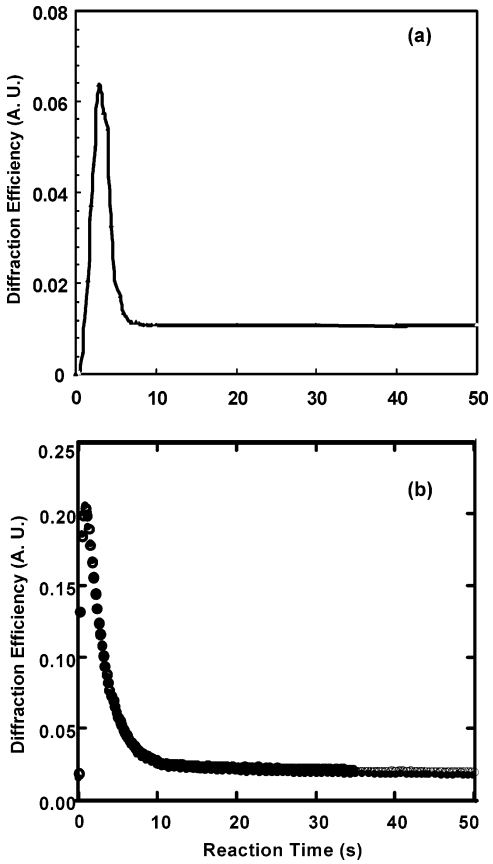

Figure 6. (a) Simulated s-polarized DE progression in 5% LC concentration sample in comparison with (b) s-polarized DE progression in 5% LC concentration sample determined experimentally from P-DSC.

the DE results of the 5% LC composition. It is promising to see the consistent trend of the evolution of the DE efficiency of the experiment and theoretical simulation, although one cannot completely rule out other effects such as incomplete reaction, reaction heat liberation, and light attenuation through film thickness.

Conclusions

The apparent reaction kinetic constants of photocurable monomer (tetraacrylate) were measured via P-DSC and FTIR. Good agreement was found between the apparent reaction kinetic constants from P-DSC and FTIR measurements. Further P-DSC experiments in samples of different ratios of tetraacrylate/LC revealed that apparent kinetic constant is not only time-dependent but also concentration-dependent. Incorporating the experimentally determined time−concentration-dependent reaction kinetic constant into the simulation of diffraction efficiency progression during H-PDLC formation, we are able to elucidate most experimental trends observed in the diffraction efficiency measurement in the 35% and 50% LC samples, especially 5% LC sample whose DE evolution is quite different from those of the 35% and 50% LC samples. It may be inferred from our simulation that the reaction kinetics on H-PDLC formation and the progression of DE are affected profoundly by the types of diffusion such as the Fick diffusion, but to a lesser extent by the mutual diffusion driven by thermodynamic force of phase separation via nucleation and growth or spinodal decomposition.

Acknowledgment. Support from the National Science Foundation through Grant DMR 0514942, the Collaborative Center for Polymer Photonics, sponsored by Air Force Office

of Scientific Research, Wright-Patterson Air Force Base, and University of Akron, and Akron Global Polymer Academy (AGPA) is gratefully acknowledged.

References and Notes

(1) Odian, G. *Principles of Polymerization*, 2nd ed.; Wiley-Interscience: New York, 1981.
(2) Andrzejewska, E. *Prog. Polym. Sci.* **2001**, *26*, 605 and references therein.
(3) Fouassier, J. P. *Photoinitiators, Photopolymerization, and Photocuring-Fundamentals and Applications*; Hauser: Munich, 1995.
(4) Kloosterboer, J. G. *Adv. Polym. Sci.* **1988**, *84*, 1.
(5) Sastre, R.; Conde, M.; Mateo, J. L. *J. Photochem. Photobiol. A: Chem.* **1988**, *44*, 11.
(6) Anseth, K. S.; Newman, S. N.; Bowman, C. N. *Adv. Polym. Sci.* **1995**, *122*, 177.
(7) Hiratani, H.; Mizutani, Y.; Alvarez-Lorenzo, C. *Macromol. Biosci.* **2005**, *5*, 728.
(8) Roffery, C. G. *Photopolymerization of Surface Coatings*; Wiley-Interscience: New York, 1982.
(9) Pappav, P. *Radiation Curing, Science and Techonology*; Plenum Press: New York, 1992.
(10) Campbell, M.; Sharp, D. N.; Harrision, M. T.; Denning, R. G.; Turberfield, A. J. *Nature (London)* **2000**, *404*, 53.
(11) Bunning, T. J.; Natarajan, L. V.; Tondiglia, V. P.; Sutherland, R. L.; Vezie, D. L.; Adams, W. W. *Polymer* **1995**, *36*, 2699.
(12) Sarkar, M. D.; Gill, N. L.; Whitehead, J. B.; Crawford, G. P. *Macromolecules* **2003**, *30*, 630.
(13) Bosch, P.; Serrano, J.; Mateo, J. L.; Calle, P.; Sieiro, C. *J. Polym. Sci., Polym. Chem.* **1998**, *36*, 2775.
(14) Hodd, K. A.; Menon, N. *Proc. Eur. Symp. Therm. Anal.* **1981**, *2nd*, 259.
(15) Hoyle, C. E.; Hensel, R. D.; Grubb, M. B. *J. Polym. Sci., Polym. Chem. Ed.* **1984**, *22*, 1865.
(16) Nelson, E. W.; Jacobs, J. L.; Scranton, A. B.; Anseth, K. S.; Bowman, C. N. *Polymer* **1995**, *36*, 4651.
(17) Nwabunma, D.; Kim, K. J.; Lin, Y.; Chien, L. C.; Kyu, T. *Macromolecules* **1998**, *31*, 6806.
(18) Soppera, O.; Croutxe-Barghorn, C. *J. Polym. Sci., Polym. Chem.* **2003**, *41*, 831.
(19) Scherzer, T.; Decker, C. *Nucl. Instrum. Methods Phys. Res. B* **1999**, *151*, 306.
(20) Decker, C.; Moussa, K. *Macromolecules* **1989**, *22*, 4455.
(21) Lee, T. Y.; Roper, T. M.; Jonsson, E. S.; Kudyakov, I.; Viswanathan, K.; Nason, C.; Guymon, C. A.; Hoyle, C. E. *Polymer* **2003**, *44*, 2859.
(22) Tryson, G. R.; Shultz, A. R. *J. Polym. Sci.* **1979**, *17*, 2059.
(23) Shultz, A. R.; Joshi, M. G. *J. Polym. Sci., Polym. Phys.* **1984**, *22*, 1753.
(24) Wen, M.; McCormick, A. V. *Macromolecules* **2000**, *33*, 9247.
(25) Perry, M. F.; Young, G. W. *Macromol. Theory Simul.* **2005**, *14*, 26.
(26) Guymon, C. A.; Bowman, C. N. *Macromolecules* **1999**, *30*, 1594.
(27) Goodner, M. D.; Bowman, C. N. *Chem. Eng. Sci.* **2002**, *57*, 887.
(28) Carre, C.; Lougnot, D. J.; Fouassier, J. P. *Macromolecules* **1989**, *22*, 791.
(29) Meng, S.; Kyu, T.; Natarajan, L. V.; Tondiglia, V. P.; Sutherland, R. L.; Bunning, T. J. *Macromolecules* **2005**, *38*, 4844.
(30) Meng, S.; Kumar, N.; Kyu, T.; Natarajan, L. V.; Tondiglia, V. P.; Bunning, T. J. *Macromolecules* **2004**, *37*, 3792.
(31) Valdes-Aguilera, O.; Pathak, C. P.; Shi, J.; Watson, D.; Neckers, D. C. *Macromolecules* **1992**, *25*, 541.
(32) Sutherland, R. L.; Tondiglia, V. P.; Natarajan, L. V.; Bunning, T. J. *Appl. Phys. Lett.* **2001**, *79*, 1420.
(33) Flory, P. J. *J. Chem. Phys.* **1942**, *10*, 51.
(34) Huggins, M. L. *J. Chem. Phys.* **1941**, *9*, 440.
(35) Boots, H. M. J.; Kloosterboer, J. G.; Serbutoviez, C.; Touwslager, F. J. *Macromolecules* **1996**, *69*, 7683.
(36) Maier, W.; Saupe, A. *Z. Naturforsch. A: Phys. Sci.* **1958**, *13a*, 564.
(37) Anseth, K. S.; Wang, C. M.; Bowman, C. N. *Macromolecules* **1994**, *27*, 650.
(38) Kogelnik, H. *Bell Syst. Tech. J.* **1969**, *48*, 2909.
(39) Montemezzani, G.; Zgonik, M. *Phys. Rev. E* **1997**, *55*, 1035.
(40) Sutherland, R. L.; Tondiglia, V. P.; Natarajan, L. V.; Bunning, T. J. *J. Appl. Phys.* **2004**, *96*, 951.
(41) Sutherland, R. L.; Natarajan, L. V.; Tondiglia, V. P.; Bunning, T. J. *Chem. Mater.* **1993**, *5*, 1533.

MA070135Q